Monthly Notices
of the
ROYAL ASTRONOMICAL SOCIETY

MNRAS **471,** 4579–4586 (2017)
Advance Access publication 2017 July 17

doi:10.1093/mnras/stx1795

# Limits on the mass, velocity and orbit of PSR J1933−6211

E. Graikou,[1⋆] J. P. W. Verbiest,[1,2] S. Osłowski,[1,2,4] D. J. Champion,[1] T. M. Tauris,[1,3] F. Jankowski[4,5] and M. Kramer[1,6]

[1]*Max-Planck-Institut für Radioastronomie, Auf dem Hügel 69, D-53121 Bonn, Germany*
[2]*Fakultät für Physik, Universität Bielefeld, Postfach 100131, D-33501 Bielefeld, Germany*
[3]*Argelander-Institut für Astronomie, Universität Bonn, Auf dem Hügel 71, D-53121 Bonn, Germany*
[4]*Centre for Astrophysics and Supercomputing, Swinburne University of Technology, PO Box 218, Hawthorn, Victoria 3122, Australia*
[5]*ARC Centre of Excellence for All-Sky Astrophysics (CAASTRO)*
[6]*Jodrell Bank Centre for Astrophysics, The University of Manchester, Manchester, M13 9PL, UK*

Accepted 2017 July 13. Received 2017 July 11; in original form 2017 June 16

## ABSTRACT

We present a high-precision timing analysis of PSR J1933−6211, a millisecond pulsar with a 3.5 ms spin period and a white dwarf (WD) companion, using data from the Parkes radio telescope. Since we have accurately measured the polarization properties of this pulsar, we have applied the matrix template matching approach in which the times of arrival are measured using full polarimetric information. We achieved a weighted root-mean-square timing residuals of the timing residuals of 1.23 μs, 15.5 per cent improvement compared to the total intensity timing analysis. After studying the scintillation properties of this pulsar, we put constraints on the inclination angle of the system. Based on these measurements and on $\chi^2$ mapping we put a $2\sigma$ upper limit on the companion mass (0.44 $M_\odot$). Since this mass limit cannot reveal the nature of the companion, we further investigate the possibility of the companion to be a He WD. Applying the orbital period-mass relation for such WDs, we conclude that the mass of a He WD companion would be about 0.26±0.01 $M_\odot$, which combined with the measured mass function and orbital inclination limits, would lead to a light pulsar mass $\leq 1.0\ M_\odot$. This result seems unlikely based on current neutron star formation models and we therefore conclude that PSR J1933−6211 most likely has a CO WD companion, which allows for a solution with a more massive pulsar.

**Key words:** pulsars: general – pulsars: individual: PSR J1933−6211.

## 1 INTRODUCTION

Millisecond pulsar (MSPs) are rapidly rotating neutron stars that have spin periods shorter than ∼30 ms. It is thought that they obtain their short spin periods from angular-momentum increases during mass transfer from their companions (Bisnovatyi-Kogan & Komberg 1974; Alpar et al. 1982). The majority of MSPs have white dwarf (WD) companions which can be either massive CO or ONeMg WDs or lower mass He WDs. CO or ONeMg WD companions are less common in binary MSPs (BMSPs), originating from intermediate-mass progenitor stars which transfer their envelope mass on a short time leaving a partly recycled MSP (with a spin period of a few tens of ms; Tauris 2011). In contrast, He WD companions are the most common and originate in low-mass X-ray binaries (LMXBs). Their time-scale of evolution is long enough to allow significant amounts of matter to accrete on to the pulsar and to fully recycle them to spin periods of a few milliseconds.

PSR J1933−6211 was discovered in 2007 at the Parkes radio telescope in the high Galactic latitude survey (Jacoby et al. 2007). Soon after the discovery it was clear that the spin period was only 3.5 ms and the orbital period was 12.28 d, which in combination with the position of the pulsar in a spin period – period derivative ($P - \dot{P}$) diagram, makes this system a typical example of a BMSP (Fig. 1). Pulsars that belong to this category, along with double neutron-star systems, are the most well-studied so far. If BMSPs are formed in an LMXB, their resulting He WDs follow a tight correlation between their mass and orbital period (Savonije 1987; Tauris & Savonije 1999). This relation can be a useful tool to probe the origin of a given BMSP and place constraints on the component masses of the system. In addition, their orbital eccentricity is also predicted to be correlated with their orbital period (Phinney 1992).

Based on equation of state and evolutionary models, the minimum allowed mass for rotating neutron stars is around 0.1–0.3 $M_\odot$

⋆ E-mail: egraikou@mpifr-bonn.mpg.de

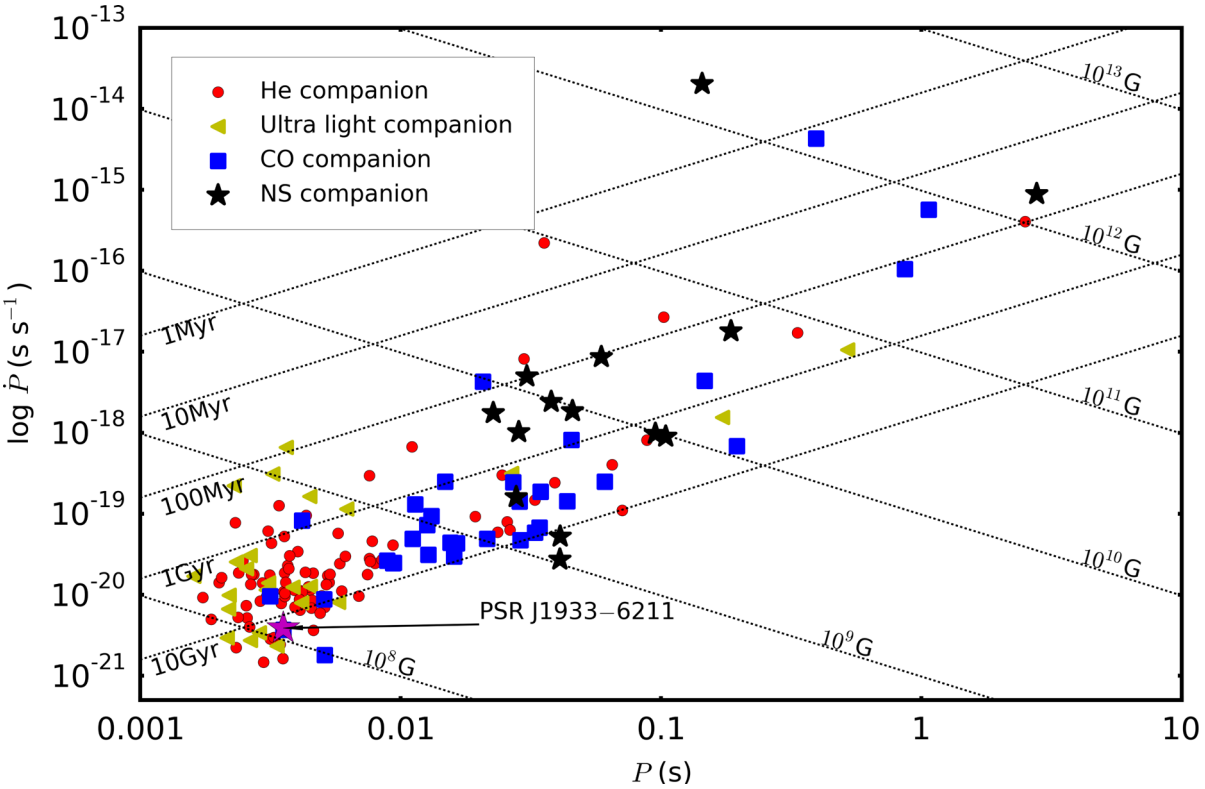


**Figure 1.** The position of PSR J1933−6211 in the period – period derivative diagram. In the plot, we present also the position of all known pulsars that have a companion. Circles indicate He WD companions, squares CO WD companions, diamonds neutron star companions and triangles ultralight or planetary companions (data taken from the ATNF Pulsar Catalogue, Manchester et al. 2005), see definition of companion stars in Tauris, Langer & Kramer (2012).

depending on their spin period (Colpi, Shapiro & Teukolsky 1993; Haensel, Zdunik & Douchin 2002). However, from current theories on stellar evolution and supernova (SN) explosion physics, minimum neutron star masses are expected to be larger than at least 1.0 $M_{\odot}$ (Timmes, Woosley & Weaver 1996). Direct pulsar mass measurements can be achieved with post-Keplerian parameter measurements through timing (Lorimer & Kramer 2012). These measurements require an eccentric, tight system, with preferably an edge-on orbit orientation. In edge-on orbits Shapiro delay detection is often possible. Shapiro delay is a time delay that arises from the photon's passage through the gravitational field of the companion star. This effect is strongest in edge-on orbits and is typically sharply peaked, with the largest delays inflicted on observations at time of superior conjunction. Efforts to measure the Shapiro delay (and thereby the companion and pulsar masses) therefore typically benefit from intense observations around superior conjunction, although full orbital coverage is typically needed to break covariances with other orbital parameters (Freire & Wex 2010).

In the cases that neither the orbit is relativistic nor the inclination of the system is high, indirect limits on the mass can be derived from the mass function. The mass function defines a relation between the Keplerian parameters with the system inclination angle and the system masses. Unlike Keplerian parameters that can be accurately measured through timing, the inclination angle and companion mass are very difficult to measure directly. In cases of close, massive WDs, optical observations, in combination with WD cooling models, may reveal the mass of the companion. When no direct measurements are feasible, pulsar timing can still be used to derive limits on the masses and orbital parameters. In those cases where the companion is a He WD, a mass estimate can be obtained from the correlation between WD mass ($M_{\rm WD}$) and orbital period ($P_{\rm b}$).

Strong scintillation of the pulsar signal can be a big observational challenge. Scintillation, which has as a result that the observed signal intensity varies, is caused by inhomogeneities and turbulence in the interstellar plasma. How strong this phenomenon is depends on the size of inhomogeneities, the distance of the pulsar, the observing frequency and the peculiar velocity. PSR J1933−6211, having a low dispersion measure of 11.520(2) pc cm$^{-3}$, is expected to scintillate strongly at 1.3 GHz frequency (Rickett 1977). Scintillation time-scale analysis can be used in order to measure the transverse velocity of the pulsar. Scintillation transverse velocity is an interstellar medium effect that is caused by the pulsar's orbital velocity, the proper motion, Earth's orbital motion, the velocity of the scattering screen and the peculiar velocity. Transverse velocity measurements allow us to put constraints on the orbital inclination of the system (Lyne 1984; Ord, Bailes & van Straten 2002) leading us to better understand the masses of the system.

In this paper, we present an updated timing analysis and mass limits for PSR J1933−6211. The observations and data reduction are described in Section 2, while the overall timing solution and the pulsar's usefulness for pulsar timing arrays (PTAs) are discussed in Section 3. Our attempts to measure the mass of this pulsar were seriously hampered by strong scintillation around the time of superior conjunction. An analysis of these scintillation measurements is given in Section 4. Next, we present the pulsar's proper motion and transverse velocity in Section 4.1. Constraints on the mass of the pulsar – and the implications for binary evolution models, are outlined in Section 5 followed by some concluding remarks in Section 6.

**Table 1.** The timing data characteristics, as observed with two different observing systems.

| | Data range (MJD) | Data range (Gregorian) | Number of ToAs | Central frequency (MHz) | Bandwidth (MHz) | Average ToA uncertainty (μs)[1] | EFAC | Weighted rms timing residual (μs) |
|---|---|---|---|---|---|---|---|---|
| CPSR2 | 52795.7–53301.4 | 2003 June–2004 October | 52 | 1341/1405 | 2 × 64 | 3.686 | 0.8/1.4 | 1.254 |
| CASPSR | 55676.0–56011.0 | 2011 April–2012 March | 96 | 1382 | 256 | 3.393 | 0.9 | 1.057 |

[1] These values correspond to the mean ToA uncertainty for 15 min integration time observations. For more typical 1 hr integrations, the ToA uncertainty (and timing rms) should decrease by up to a factor of 2.

## 2 OBSERVATIONS AND DATA REDUCTION

Our observations of PSR J1933−6211 were performed with the Parkes 64 m radio telescope. The total span is ∼10 years divided into two epochs of ∼1 year of observations each (Fig. 3). In the first epoch, the pulsar is observed as part of the high Galactic latitude survey follow-up observations (Jacoby et al. 2007). These archival data, biblically available, were recorded with the Caltech Swinburne Parkes Recorder 2 (CPSR2) coherent dedispersion backend (Hotan, Bailes & Ord 2006) that provides two dual-polarization bands of 64 MHz, each centred on 1341 and 1405 MHz, respectively. Each of the bands was split into 128 frequency channels using a polyphase filterbank.

The aim of the second epoch of observations was to precisely measure the orbital parameters of the system and the masses. The observations were performed with the CASPSR backend (Hickish et al. 2016), which provides a 256 MHz bandwidth, centred at 1382 MHz, resulting in a significant increase in sensitivity (Table 1). All the observations were taken at a wavelength of 21cm with the central beam of the Parkes multibeam receiver (Staveley-Smith et al. 1996).

Since one of our goals is to measure the system masses, we picked our observations strategy in a way that we were sensitive to Shapiro delay detection. This phenomenon maximally affects pulse arrival times at superior conjunction. Superior conjunction is the point in the orbit where the pulsar is behind its companion. Consequently we defined our observing strategy to have uniform coverage through 75 per cent of the orbit, but increased observing cadence during the 25 per cent of the orbit surrounding superior conjunction. The length of a typical observing scan was 30 min.

We divided each observation into 15 min segments. Each of these 15 min sub-integrations were weighted by their signal-to-noise (S/N) ratio before the segments were integrated in time and frequency. The observations that provided the best S/N were combined and von Mises functions were fitted in order to create an analytic template. We followed the same procedure to create templates for each of the two backends for which the data were available. We measured the pulse times-of-arrival (ToAs) with two different methods. In the first method, we correlated the analytic templates with the observations by applying goodness-of-fit statistics in the frequency domain (Taylor 1992), and in the second method we applied the matrix template matching approach for which we used the full polarization information of the pulsar signal in the template.

In order to optimise the sensitivity of our analysis, we performed full polarimetric calibration following the methods described by (van Straten 2004, 2013). Specifically, a time-dependent receiver model was derived from long-track observations of PSR J0437−4715 following the polarimetric calibration-modelling technique described by van Straten (2004). This solution was then applied to the PSR J1933−6211 data using the measurement-equation template-matching technique of van Straten (2013). The Stokes parameters in the calibrated data follow the conventions defined by van Straten et al. (2010).

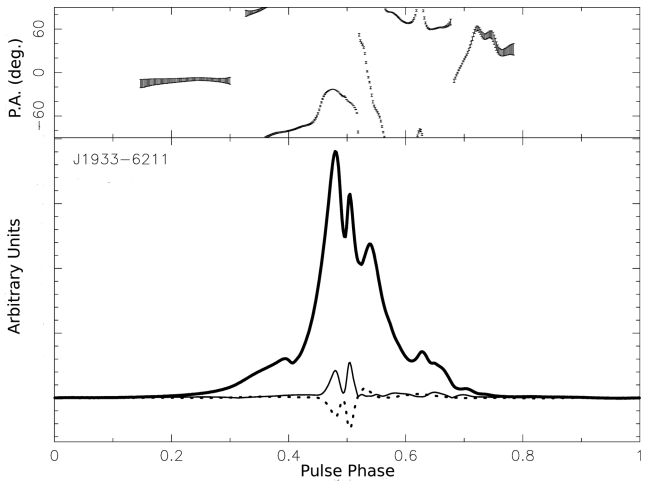


**Figure 2.** Average polarization calibrated pulse profile from the CASPSR backend data at 1382 MHz central frequency (averaged across a bandwidth of 256 MHz). In the plot, the linear (solid) and circular polarization (dotted) profiles are presented as well as the total intensity profile (bold). The flux scale is arbitrary. The fact that the main pulse is sub-divided into three individual sharp components, greatly aids the timing precision achievable in this system. This resolved main pulse was not presented in the discovery publication (Jacoby et al. 2007), which used data from the analogue filterbank, which does not perform coherent dedispersion and thereby smears out the fine structure in the pulse profile.

Based on the polarized pulse shape (see Fig. 2), we performed the analysis of van Straten (2006), which suggests a theoretical ∼ 25 per cent improvement in ToA precision, depending on the degree of polarization and the variability of the polarization vector as a function of pulse phase can be obtained if ToAs were derived by using the full polarization information (instead of deriving ToAs from the total-intensity profile only, as is common in pulsar timing). To verify this result, we derived two sets of ToAs: one set based on the total-intensity pulse profile and one based on the full polarimetric polarization, using the van Straten (2006) timing method. In the remainder of the paper we use full polarimetric polarization residuals unless otherwise stated.

The resulting phase-connected full polarimetric polarization ToA residuals are presented in Fig. 3. The comparison with the total-intensity residuals led to an overall improvement of 15.5 per cent in timing residuals and 20 per cent in ToAs uncertainty.

The packages that were used for the analysis described above are PSRCHIVE (Hotan, van Straten & Manchester 2004; van Straten, Demorest & Oslowski 2012) and TEMPO2 (Hobbs, Edwards & Manchester 2006).

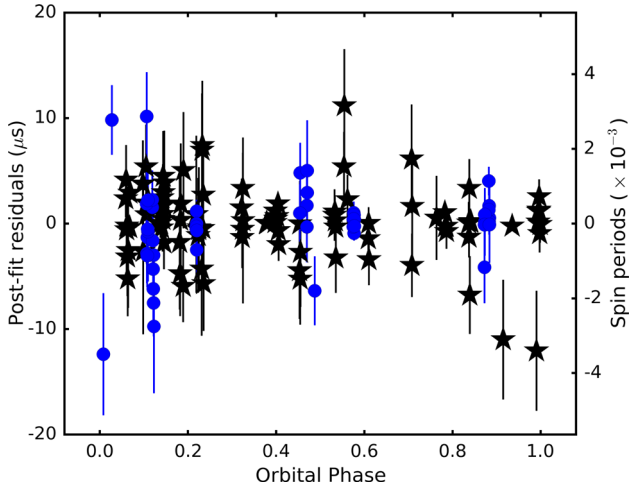


**Figure 3.** The timing residuals at 20 cm as a function of orbital phase, using the CPSR2 (circles) and CASPSR (stars) data.

## 3 TIMING SOLUTION AND HIGH-PRECISION POTENTIAL

A total of 148 ToAs were formed in order to measure the orbital, spin characteristics and the astrometry of PSR J1933−6211. Since the eccentricity of the system is very low, we applied the ELL1 model (Lange et al. 2001), for which the eccentricity, $e$, the epoch and the longitude of periastron passage, $T_0$ and $\omega$, respectively, are replaced by the Laplace–Lagrange parameters, $\eta = e \sin\omega$ and $\kappa = e \cos\omega$ and the time of the ascending node passage $T_{\rm asc}$.

We fit for pulsar parameters using least-squares fitting in order to minimize the differences between measured ToAs and the expected arrival times derived from the analytical model (Edwards, Hobbs & Manchester 2006). A phase offset was fitted between the CPSR2 and the CASPSR data account for any difference in instrumental delays. We furthermore multiplied the ToA uncertainties with error-scaling-factors (EFACs) of 0.8 and 1.4 for the data correspond to the two CPSR2 polarization bands and 0.9 CASPSR data, respectively. These factors account for any possible underestimation of the ToA uncertainties, as described in Verbiest et al. (2016). We note that the phase offset between the backends is only 1.71 μs. Given this small offset, the fact that the timing model fits both sub-sets equally well and that the fit worsens considerably when an integer number of pulse periods get either added or subtracted from this offset value, clearly indicates that phase-connection was achieved across the 6 yr gap.

The TT(BIPM(2013)) terrestrial time standard and the DE421 Solar system ephemeris were used in order to convert from topocentric to barycentre arrival times.

The resulting timing parameters that correspond to our best-fitting residuals (Fig. 3) are presented in Table 2. The timing analysis led to significant measurements of the proper motion, the spin and spin-down and the Keplerian parameters of the system. All these well-measured parameters led us to further investigate the geometry and the origin of the system.

With a weighted rms of only 1.23 μ$s$, PSR J1933−6211 is a good candidate to be added in the PTA projects that aim to detect gravitational waves in the nHz regime as its timing rms compares well to that of most sources in the international PTA (Verbiest et al. 2016).

**Table 2.** The timing parameters of the system that correspond to the best-fitting residuals.

| | |
|---|---|
| General information | |
| MJD range | 52795–53301 |
| | 55676–56011 |
| Number of ToAs | 148 |
| Weigthed rms timing residual (μs) | 1.23 |
| Measured quantities | |
| Right ascension, $\alpha$ (J2000) | 19:33:32.42668(5) |
| Declination, $\delta$ (J2000) | −62:11:46.876(1) |
| Proper motion in $\alpha$, $\mu_\alpha$ (mas yr$^{-1}$) | −5.54(7) |
| Proper motion in $\delta$, $\mu_\delta$ (mas yr$^{-1}$) | 10.7(2) |
| Total proper motion (mas yr$^{-1}$) | 12.1(2) |
| Spin frequency, $\nu$ (Hz) | 282.212 313 615 28(2) |
| Spin-down, $\dot{\nu}$ ($\times 10^{-16}$ Hz s$^{-1}$) | −3.0828(7) |
| Dispersion measure, $DM$ (pc cm$^{-3}$) | 11.520(2) |
| Orbital period, $P_{\rm b}$ (d) | 12.819 406 7183(8) |
| Time of ascending node, $T_{\rm asc}$ (MJD) | 53 000.495 2524(2) |
| Projected semimajor axis, $a_{\rm p}$=a sin$i$ (lt-s) | 12.281 5745(3) |
| $\eta = e \sin\omega$ ($\times 10^{-6}$) | 1.36(4) |
| $\kappa = e \cos\omega$ ($\times 10^{-6}$) | −0.32(3) |
| Derived quantities | |
| Epoch of periastron passage, $T_0$ (MJD) | 53004.17(5) |
| Longitude of periastron, $\omega$ (deg) | 103(1) |
| Orbital eccentricity, $e$ ($\times 10^{-6}$) | 1.40(4) |
| Mass function, $f$(M$_\odot$) | 0.0121 034(2) |
| $2\sigma$ limits from $\chi^2$ mapping | |
| Longitude of the ascending node, Ω (deg) | 4–148 |
| Companion mass, $M_{\rm wd}$ (M$_\odot$) | $< 0.44$ |
| Distance, $d$ (kpc) | $> 0.11$ |
| Assumptions | |
| Clock correction procedure | TT(BIPM(2013)) |
| Solar system ephemeris model | DE421 |
| Binary model | ELL1 |

*Note:* Figures in parentheses are the nominal 1$\sigma$ TEMPO2 uncertainties in the least-significant digits quoted.

### 3.1 Mass constraints from timing

The lack of a Shapiro delay detection and precise post-Keplerian parameter measurements, $\dot{\omega}$ and $\dot{P}_{\rm b}$, has as a result that with the current timing direct system-mass measurements are not possible. Instead, we derived constraints on the masses and orientation of the system by mapping the goodness-of-fit (as determined by the $\chi^2$ value of the fit) over a four-dimensional grid covering the companion mass $M_{\rm c}$, the inclination angle of the system $i$, the longitude of the ascending node Ω and the distance to the system $D$. At each pixel of this four-dimensional grid, these four parameters were held fixed, as were the post-Keplerian parameters $\dot{\omega}$ and $\dot{P}_{\rm b}$ that were derived from these. (Note while the distance does not enter in the post-Keplerian parameters, it was used to determine the parallax, which was kept fixed, and it entered in the calculation of the Kopeikin terms that define $i$ and Ω; Kopeikin 1995, 1996). Our grid had a step size of 0.01 M$_\odot$ in $M_{\rm c}$, 0.°01 in $i$, 1° in Ω and 20 pc in distance, so our results (see Table 2) are quantised at these levels.

In Fig. 4, our results are presented with 95 per cent confidence limit on the companion mass. The lower limit for the WD mass (0.1 M$_\odot$) comes directly from the mass function, evaluated for an edge-on orbit, provided that the pulsar mass is >0.0 M$_\odot$. These limits do not allow us to identify the companion star as either a He

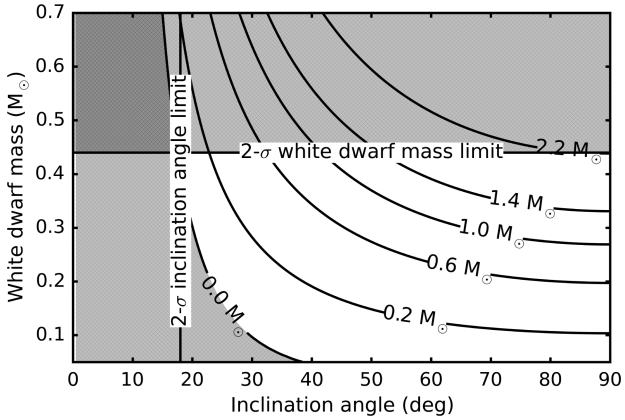


**Figure 4.** Mass-inclination angle diagram indicating the limits derived from timing. Specifically, the bottom-left region is excluded by the mass function and the requirement that $M_{\rm psr} > 0$ and the $2\sigma$ upper limit on the companion mass, derived from our goodness-of-fit mapping, is indicated by the horizontal line at $M_{\rm c} = 0.44\ {\rm M}_\odot$ (see Section 3.1).

or CO WD. In Section 5, we revisit this question based on some alternative, more theoretical, approaches.

### 3.2 Characteristic age

The age of pulsars is key for evolutionary models. But in order to measure it precisely, we should know the pulsar's spin period at birth and the braking index. In order to approximate this problem we make some assumptions: the initial period of a pulsar is much lower than the one that we measure today, and the pulsar loses energy due to magnetic dipole radiation with a constant B-field (braking index equal to three). We can then estimate the characteristic age $\tau$

$$\tau = \frac{P}{2\,\dot{P}}, \qquad (1)$$

which is only a rough estimate of the real age (see below).

PSR J1933−6211 has a very low spin period derivate, as derived from timing (see Table 2). For pulsars with such low spin period derivates, effects like the Shklovskii effect and Galactic acceleration can have a significant impact on the observed spin period derivative. In order to calculate more accurately the characteristic age, we measured the contribution of these kinematic effects in $\dot{P}$.

Both effects are quite small in PSR J1933−6211, the Shklovskii effect that is calculated from

$$\left(\frac{\dot{P}}{P}\right)_{\rm Shk} = 2.43 \times 10^{-21}\ \frac{\mu^2}{({\rm mass\ yr^{-1}})}\ \frac{d}{({\rm kpc})}, \qquad (2)$$

is $1.8(3) \times 10^{-19}$ s s$^{-1}$.

The Galactic acceleration contribution is defined by:

$$\left(\frac{\dot{P}}{P}\right)_{\rm Gal\ acc} = \frac{\alpha_z \sin b}{\rm c} - \cos b \left(\frac{\Theta_0^2}{\rm cR_0}\right)\left(\cos l + \frac{\beta}{\sin^2 l\ +\ \beta^2}\right), \qquad (3)$$

where the Galactic distance of the Solar system: $\rm R_0 = 8.34\,kpc$, the circular rotation speed of the Galaxy at $\rm R_0$: $\Theta_0 = 240\,km\,s^{-1}$ (Reid et al. 2014), $l$ the Galactic longitude, $b$ the Galactic latitude and $\beta = (d/{\rm R_0})\cos b - \cos l$. It is measured to be: $9.6(6) \times 10^{-20}$ s s$^{-1}$. The resulting characteristic age after taken into account these effects is 14.6(4) Gyr, which exceeds the Hubble time. Such large characteristic ages have been pointed out before (Camilo, Thorsett & Kulkarni 1994), and are caused by the fact that the spin period derivate is too small to cause rapid changes in the pulsar spin period, so we observe the pulsar almost at its birth $P$ and $\dot{P}$ values (Tauris et al. 2012), and thus equation (1) above brakes down since it assumes $P_0 \ll P$, where $P_0$ is the birth spin period (after accretion). Instead, for MSPs the value of $\tau$ is a measure of its remaining lifetime as a radio pulsar.

## 4 SCINTILLATION MEASUREMENTS

During our observations we measured strong scintillation. The mean S/N for observations that are fully averaged in time and frequency and polarization calibrated, is 29, but reaches ∼200 during scintillation maxima, for 15 min observation scans, a factor of almost seven stronger.

We managed to observe only two complete scintles due to the length of the scintillation time-scale and the fact that the individual observations were conventionally ∼30 min long. For the scintillation analysis we used only CASPSR data with 5 min integrations divided into 512 frequency channels (over a 256 MHz bandwidth). For each observation we removed the band edges, which corresponds to 10 per cent of the band. We manually cleaned the remaining radio frequency interference (RFI) for the cases where it was needed.

In order to measure the scintillation time-scale and bandwidth we fitted one-dimensional Gaussian functions to the frequency (respectively time) averaged intensity series of the dynamical spectrum. The number of Gaussians that are used to fit the data has been decided through a Kolmogorov–Smirnov test by requiring the post-fit intensities to follow a Gaussian distribution with 95 per cent certainty (see Fig. 5). In Table 3, we present the scintillation parameters for the two available scintles as derived from the method that we explained above.

The scintillation properties allow transverse velocity measurements. The comparison with theoretical transverse velocity and further inclination angle limits are presented below.

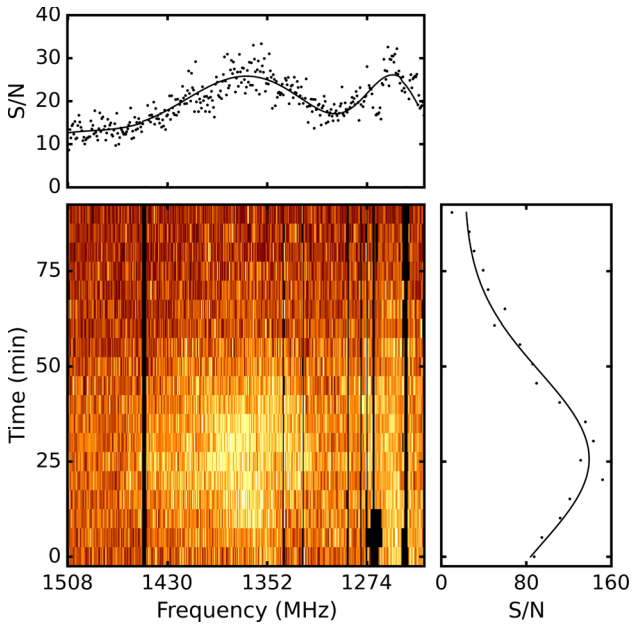


**Figure 5.** Dynamic spectrum of a full scintle of PSR J1933−6211 as observed on 2011 May 16. In the top and right plots, the S/N in each frequency channel and in each sub-integration are presented, respectively. The solid line corresponds to a Gaussian fitting line to our observation.

**Table 3.** Scintillation parameters and the derived scintillation speed of the two complete scintles. Both observations were taken with the CASPSR backend at 1382 MHz central frequency with 256 MHz observing bandwidth divided into 512 channels and 5 min time resolution.

| Data | 2011-05-03 | 2011-05-16 |
|---|---|---|
| $\Delta t$ (min) | 181(5) | 108(5) |
| $\Delta f$ (MHz) | 358(8) | 155(8) |
| $V_{\rm ISS}$ based on NE2001 (km s$^{-1}$) | 34(3) | 38(3) |
| Orbital phase ($\phi$) | 0.2 | 0.2 |

### 4.1 Transverse velocity and inclination angle limit

Various studies have investigated the space velocity of pulsars. Desvignes et al. (2016), after investigating 42 MSPs pulsars, concluded that the mean transverse velocities of MSPs is 92±10 km s$^{-1}$, a factor of 4 lower than that of young pulsars (Hobbs et al. 2005). This difference can be understood from their dissimilar kick velocities at birth. Such a differentiation is thought to arise from a combination of different masses of the exploding stars forming neutron stars in isolation versus in close binaries (the latter being stripped prior to the explosion) and the absorption of the kick momentum in a binary system (Tauris & Bailes 1996). Newborn pulsars are expected to receive a broad range of kicks – between 0 and more than 1000 km s$^{-1}$ (Janka 2016). The binaries that eventually give rise to MSPs, survived the SN kick, which could mean that the kick often was either small or fortuitously oriented.

Pulsar space velocities can be measured through scintillation properties of the pulsar. By assuming that the diffraction screen is located in the middle between the Earth and the pulsar and that the scattering medium is a uniform Kolmogorov medium, we calculate the scintillation speed from (Gupta, Rickett & Lyne 1994)

$$V_{\rm ISS}({\rm km\ s^{-1}}) \;=\; 3.85\times10^{4}\;\frac{\sqrt{d({\rm kpc})\;\Delta f({\rm MHz})}}{f({\rm GHz})\;\Delta t({\rm s})}, \qquad (4)$$

where $d$ is the distance of the pulsar, $f$ is the observing frequency and $\Delta f$ and $\Delta t$ are the scintillation bandwidth and time-scale (see Table 3).

The dispersion measure can give an estimate of the pulsar distance. We consider two such distances derived from two different models: the widely used NE2001 model (Cordes & Lazio 2002) and the most recent YMW16 model (Yao, Manchester & Wang 2017). The NE2001 model has been widely scrutinised whenever new pulsar distances were measured (see e.g. Desvignes et al. 2016; Matthews et al. 2016), leading to the conclusion that for pulsars at low and medium Galactic latitudes this model gives a good distance prediction, comparable to pulsar parallax measurements. For PSR J1933−6211 with Galactic latitude of −28.°6315 and a dispersion measure equal to 11.520(2) pc cm$^{-3}$ the model-predicted distance is 0.51(7) kpc and 0.65 kpc based on NE2001 and YMW16, respectively. The scintillation speed that we measured based on NE2001 distance measurements is equal to 36(2) km s$^{-1}$.

The pulsar space velocity ($V_{\rm model}$), that we measured through scintillation speed, is composed of the pulsar's orbital velocity ($V_{\rm orb}$), proper motion ($V_{\rm pm}$), Earth's velocity ($V_{\rm Earth}$) and the velocity of the scattering screen ($V_{\rm ISM}$).

$$V_{\rm model} \;=\; \underbrace{V_{\rm orb}}_{\alpha_{\rm p},\,P_{\rm b},\,\omega,\,i,\,e,\,\phi} \;+\; \underbrace{V_{\rm pm}}_{\Omega,\,d,\,\mu_{\alpha},\,\mu_{\delta}} \;+\; V_{\rm Earth} \;+\; V_{\rm ISM} \qquad (5)$$

The proper motion and the orbital velocity, that either added or subtracted to the proper motion, contribute the most to the pulsar space velocity, since $V_{\rm ISM}$ can be neglected (Gupta 1995) and $V_{\rm Earth}$ is considered as constant throughout the observation. Since the pulsar is moving, as we observe if we track it in different positions on the sky, having as a result to detect differences in $V_{\rm ISS}$. By monitoring these changes in respect to orbital phase, we can obtain useful information about the geometry of the system. For example, Lyne (1984) and Ord et al. (2002) measured the inclination angles of the PSR B0655+64 and J1141−6545 systems, respectively, based on the orbital dependence of the scintillation speed. Unfortunately, based on our analysis, the fact that both scintles are detected at the same orbital phase (Table 3), didn't allow us to perform a $\chi^2$ mapping in order to put constraints on the inclination angle of the system. Luckily, we can further investigate the geometry of the system based on the timing constraints on the longitude of the ascending node ($\Omega$, see Section 3.1 and Table 2 ).

We compared the scintillation speed, measured with our data (Table 3), with the model of the pulsar space velocity (equation 5). The $\omega$, $P_{\rm b}$, $e$, $\alpha_{\rm p}$ and proper motion can be accurately measured through timing (Table 2). Our unknowns are two: $\Omega$ and $i$. The measured orbital velocity depends only on the unknown inclination angle

$$V_{\rm orb} \;=\; \frac{2\,\pi\,a_{\rm p}}{\sin i\sqrt{1-e^2}P_{\rm b}} \;=\; \frac{20.886\;8501(5)}{\sin\,i}\ {\rm km\ s^{-1}}. \qquad (6)$$

Higher inclination angles correspond to lower orbital velocities and as a result to lower observed scintillation speeds. The highest probable orbital velocity that can be measured for this system, in the 0.2 orbital phase, is ∼120 km s$^{-1}$ and the lowest is ∼2 km s$^{-1}$.

The other unknown is $\Omega$ for which we have a $2\sigma$ limit through timing (see Table 2). Inside this $\Omega$ $2\sigma$ parameter space we find the $i$ values for which the $V_{\rm model}$ is consistent to our scintillation speed based on our observations. Our results are presented in Fig. 6. The fact that two regions of $i$ are allowed, is due to the 180 degree ambiguity in $\Omega$, raised from the fact that we can not determine which of the two orbit nodes is the ascending node.

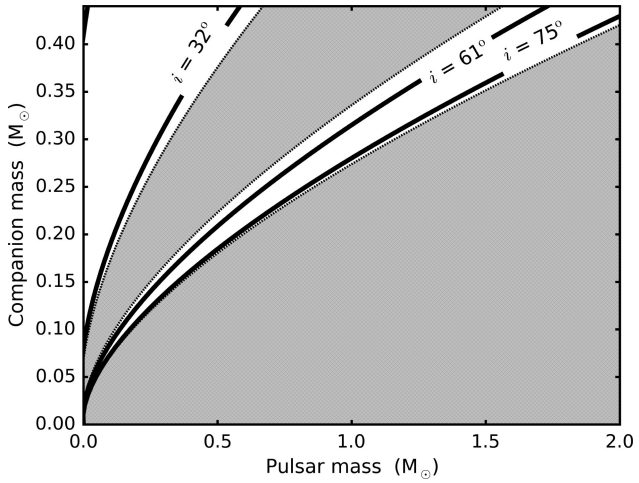


**Figure 6.** Pulsar mass – companion mass diagram. The grey areas indicate inclination angles excluded with $1\sigma$. With the solid lines, the inclination angle $1\sigma$ limits for this system are presented, as measured based on the scintillation speed. With the dotted lines the error is presented. Our two sets of solutions arise from the fact that we cannot determine which of the two nodes is the ascending node.

**Table 4.** WD mass estimates assuming different chemical compositions of its progenitor star, based on the orbital period – WD mass relation for He WD companions (Tauris & Savonije 1999) and given that $P_b = 12.8$ d for PSR J1933−6211.

| Population | WD mass ($M_\odot$) |
|---|---|
| I | 0.251 |
| I & II | 0.264 |
| II | 0.277 |

## 5 LIMITS ON THE SYSTEM MASSES

In addition to the timing-based constraints presented in Section 3.1, for LMXBs, there are theoretical relations between the orbital parameters and the pulsar and companion masses. We will now consider these theoretical models and their predictions, in order to investigate the nature of the WD companion.

### 5.1 Orbital eccentricity

Phinney & Kulkarni (1994) found a relationship between the orbital eccentricity and orbital period for cases where the pulsar is formed after stable mass transfer in an LMXB from a red giant filling its Roche lobe. For orbital periods of 12.8 d, the 95 per cent lower limit on the eccentricity as predicted from this model is significantly higher than the value that we derived from timing (Table 2). This discrepancy is caused by the uncertainty in input physics applied for the modelling, i.e. related to tidal interactions and convection in the outer layers of the progenitor star. As a result, there is a large scatter in eccentricities for observed BMSPs with a given orbital period (cf. Fig. 4 in Tauris et al. 2012).

### 5.2 Orbital period – WD mass relation

Different studies have investigated the relationship between the orbital period and the companion mass in MSP – WD binaries which originate from LMXBs (Savonije 1987; Rappaport et al. 1995; Tauris & Savonije 1999; Istrate, Tauris & Langer 2014). This relation has its basis in a correlation between the radius of a low-mass red giant star and the mass of its degenerate He core.

Numerical stellar evolution calculations have been done by Tauris & Savonije (1999) to investigate this relationship for LMXBs with wide orbits (>2 d). Based on computations of dynamically stable mass transfer in LMXBs, they obtained a relationship between the orbital period and the WD mass for different chemical compositions of the donor star. Based on this analysis, the derived WD mass varies from 0.251 to 0.277 $M_\odot$ (Table 4).

The mass of the WD is related to the mass of the neutron star ($M_{ns}$) and the orbital inclination angle ($i$) through the mass function

$$f(M) = (M_{wd} \sin i)^3/(M_{ns} + M_{wd})^2, \quad (7)$$

In Fig. 7 we present this relation for three different WD masses, see Table 4 above. The derived upper limit for the neutron star mass is $0.96 \pm 0.08$ $M_\odot$. This very low pulsar mass limit, can be even lower if we combine it with the inclination angle limit: $i < 80^\circ$, as calculated based on the scintillation speed measurements. Neutron star masses lower than 1.1 $M_\odot$ are not consistent with theoretical models of their formation (Timmes et al. 1996). For this reason it is very unlikely that the WD companion would be a He WD, and therefore we suggest that this system did not originate from an LMXB. Hence, the WD probably has a larger mass (and quite likely a CO composition), which also implies a larger mass of the neutron star.

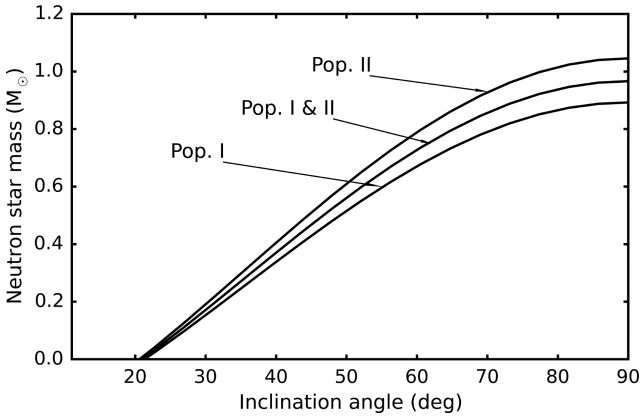


**Figure 7.** PSR J1933−6211 mass estimate as a function of inclination angle based on the theoretical orbital period – WD mass relations for He WD companions (see Section 5.2). The three neutron star mass lines are based on different chemical compositions of the progenitor star of the WD (Table 4).

The formation of a fully recycled MSP, like PSR J1933−6211, requires mass transfer on a long time-scale which, until the discovery of PSR J1614−2230 (Hessels et al. 2005), has only been explained through an LMXB evolution. The discovery of the PSR J1614−2230 system brought a paradox, since the pulsar is an MSP with spin period 3.2 ms and yet it has a CO WD companion (Demorest et al. 2010). The formation of PSR J1614−2230 is explained with an intermediate-mass X-ray binary (IMXB) which evolved from Case A Roche lobe overflow (RLO) (Tauris, Langer & Kramer 2011; Lin et al. 2011). Another recently discovered candidate member of this class is PSR J1101−6424 (Ng et al. 2015). In the formation scenario of these systems, the RLO begins when the progenitor of the WD is still on the main sequence (i.e. undergoing core hydrogen burning) and therefore the time-scale of the RLO is relatively long, such that the amount of mass that is transferred to the neutron star is sufficient to form an MSP. In case of IMXBs in a close orbit, the mass of the remnant CO WD can be as low as 0.33 $M_\odot$ (Kippenhahn & Weigert 1990; Tauris, van den Heuvel & Savonije 2000). This limit is consistent with our $2\sigma$ WD upper limit of 0.44 $M_\odot$ derived from timing (Fig. 4). Finally, we note that the orbital period of PSR J1933−6211 (12.8 d) is also consistent with an IMXB forming a CO WD companion (Tauris et al. 2000). For optical constraints on the WD companion in PSR J1933−6211, see Mateo et al. (in preparation).

## 6 CONCLUSIONS

We have presented high-precision timing of PSR J1933−6211, a MSP with a WD companion, using the Parkes radio telescope. After applying the matrix template matching technique we managed to achieve ToAs precision of 1.23 $\mu s$ and we reached an improvement of 15.5 per cent in timing residuals, compared to the total intensity timing analysis. We determined precise spin and spin derivative values and the orbital parameters of the system.

The two scintles that we observed allowed us to determinate the scintillation parameters of the system. This information leads us to transverse velocity measurements of 26(2) km $s^{-1}$. Based on $\Omega$ $1\sigma$ limits, obtained from $\chi^2$ mapping, the Keplerian parameters, measured through timing, and the transverse velocity we put

limits on the inclination angle of the system. We concluded that the inclination angle is likely lower than $\sim 80^{\circ}$.

The lack of Shapiro delay, $\dot{\omega}$ and $\dot{P}_{\rm p}$ measurements prevents direct mass measurements. For this reason, we performed $\chi^2$ mapping in order to put limits on the WD mass. Our $2\sigma$ upper limit for the WD mass is 0.44 $M_{\odot}$. This limit corresponds to 2.2 $M_{\odot}$ as an upper pulsar mass limit for a high inclination angle. Based on this limit, we cannot distinguish between the possibility of a CO or a He WD. For this reason, we further investigated the possibility that the companion is a He WD. These type of MSP systems are very well studied. Based on the orbital period – WD mass relationship resulting from LMXB evolution (Tauris & Savonije 1999), we derived an upper limit for the pulsar mass of $0.96 \pm 0.08$ $M_{\odot}$. Therefore, we conclude that if PSR J1933−6211 has indeed a He WD companion then the mass of the pulsar is very light – in fact, too light to be consistent with current stellar evolution and SN explosion physics modelling. We therefore, conclude that the companion of PSR J1933−6211 is most likely a CO WD, and therefore this system has an origin in an IMXB system, somewhat similar to the BMSP J1614−2230.

## ACKNOWLEDGEMENTS

We would like to thank Aidan Hotan and Matthew Bailes for their observing support and Willem van Straten for useful discussions. The observations were performed with the Parkes radio telescope: The Parkes Observatory is part of the Australian Telescope which is funded by the Commonwealth of Australia for operation as a National Facility managed by Commonwealth Scientific and Industrial Research Organisation (CSIRO). Parts of this research were conducted by the Australian Research Council Centre of Excellence for All-sky Astrophysics (CAASTRO), through project number CE110001020. EG acknowledges the support from International Max Planck Research School (IMPRS) Bonn/Cologne and the Bonn–Cologne Graduate School (BCGS). SO acknowledges support from the Alexander von Humboldt Foundation and Australian Research Council grant Laureate Fellowship FL150100148.

## REFERENCES

Alpar M. A., Cheng A. F., Ruderman M. A., Shaham J., 1982, Nature, 300, 728
Bisnovatyi-Kogan G. S., Komberg B. V., 1974, Soviet Astron., 18, 217
Camilo F., Thorsett S. E., Kulkarni S. R., 1994, ApJ, 421, L15
Colpi M., Shapiro S. L., Teukolsky S. A., 1993, ApJ, 414, 717
Cordes J. M., Lazio T. J. W., 2002, preprint (astro-ph/0207156)
Demorest P. B., Pennucci T., Ransom S. M., Roberts M. S. E., Hessels J. W. T., 2010, Nature, 467, 1081
Desvignes G. et al., 2016, MNRAS, 458, 3341
Edwards R. T., Hobbs G. B., Manchester R. N., 2006, MNRAS, 372, 1549
Freire P. C. C., Wex N., 2010, MNRAS, 409, 199
Gupta Y., 1995, ApJ, 451, 717
Gupta Y., Rickett B. J., Lyne A. G., 1994, MNRAS, 269, 1035
Haensel P., Zdunik J. L., Douchin F., 2002, A&A, 385, 301
Hessels J., Ransom S., Roberts M., Kaspi V., Livingstone M., Tam C., Crawford F., 2005, in Rasio F. A., Stairs I. H., eds, ASPacific Conf. Ser. Vol. 328, Binary Radio Pulsars. Astron. Soc. Pac., San Francisco, p. 395
Hickish J. et al., 2016, J. Astron. Instrum., 5, 1641001
Hobbs G., Lorimer D. R., Lyne A. G., Kramer M., 2005, MNRAS, 360, 974
Hobbs G. B., Edwards R. T., Manchester R. N., 2006, MNRAS, 369, 655
Hotan A. W., van Straten W., Manchester R. N., 2004, Publ. Astron. Soc. Australia, 21, 302
Hotan A. W., Bailes M., Ord S. M., 2006, MNRAS, 369, 1502
Istrate A. G., Tauris T. M., Langer N., 2014, A&A, 571, A45
Jacoby B. A., Bailes M., Ord S. M., Knight H. S., Hotan A. W., 2007, ApJ, 656, 408
Janka H.-T., 2016, ApJ, 837, 84
Kippenhahn R., Weigert A., 1990, Stellar Structure and Evolution. Springer-Verlag, Berlin
Kopeikin S. M., 1995, ApJ, 439, L5
Kopeikin S. M., 1996, ApJ, 467, L93
Lange C., Camilo F., Wex N., Kramer M., Backer D. C., Lyne A. G., Doroshenko O., 2001, MNRAS, 326, 274
Lin J., Rappaport S., Podsiadlowski P., Nelson L., Paxton B., Todorov P., 2011, ApJ, 732, 70
Lorimer D. R., Kramer M., 2012, Handbook of Pulsar Astronomy. Cambridge Univ. Press, Cambridge
Lyne A. G., 1984, Nature, 310, 300
Manchester IV, W. B. et al., 2005, ApJ, 622, 1225
Matthews A. M. et al., 2016, ApJ, 818, 92
Ng C. et al., 2015, MNRAS, 450, 2922
Ord S. M., Bailes M., van Straten W., 2002, ApJ, 574, L75
Phinney E. S., 1992, Phil. Trans. R. Soc. A, 341, 39
Phinney E. S., Kulkarni S. R., 1994, ARA&A, 32, 591
Rappaport S., Podsiadlowski P., Joss P. C., Di Stefano R., Han Z., 1995, MNRAS, 273, 731
Reid M. J. et al., 2014, ApJ, 783, 130
Rickett B. J., 1977, ARA&A, 15, 479
Savonije G. J., 1987, Nature, 325, 416
Staveley-Smith L. et al., 1996, Publ. Astron. Soc. Australia, 13, 243
Tauris T. M., 2011, in Schmidtobreick L., Schreiber M. R., Tappert C., eds, ASP Conf. Ser. Vol. 447, Evolution of Compact Binaries. Astron. Soc. Pac., San Francisco, p. 285
Tauris T. M., Bailes M., 1996, A&A, 315, 432
Tauris T. M., Savonije G. J., 1999, A&A, 350, 928
Tauris T. M., van den Heuvel E. P. J., Savonije G. J., 2000, ApJ, 530, L93
Tauris T. M., Langer N., Kramer M., 2011, MNRAS, 416, 2130
Tauris T. M., Langer N., Kramer M., 2012, MNRAS, 425, 1601
Taylor J. H., 1992, Phil. Trans. R. Soc. A, 341, 117
Timmes F. X., Woosley S. E., Weaver T. A., 1996, ApJ, 457, 834
van Straten W., 2004, ApJS, 152, 129
van Straten W., 2006, ApJ, 642, 1004
van Straten W., 2013, ApJS, 204, 13
van Straten W., Manchester R. N., Johnston S., Reynolds J. E., 2010, Publ. Astron. Soc. Australia, 27, 104
van Straten W., Demorest P., Oslowski S., 2012, Astron. Res. Technol., 9, 237
Verbiest J. P. W. et al., 2016, MNRAS, 458, 1267
Yao J. M., Manchester R. N., Wang N., 2017, ApJ, 835, 29

This paper has been typeset from a TEX/LATEX file prepared by the author.